Research Article | Vol. 25, No. 1 | 9 Jan 2017 | OPTICS EXPRESS 320

Optics EXPRESS

Characterization and adaptive compression of a multi-soliton laser source

GENNADY RASSKAZOV,[1,4] ANTON RYABTSEV,[1,4] KRITI CHARAN,[2] TIANYU WANG,[2] CHRIS XU,[2] AND MARCOS DANTUS[1,3,*]

[1]*Department of Chemistry, Michigan State University, East Lansing, MI 48824, USA*
[2]*School of Applied and Engineering Physics, Cornell University, Ithaca, NY 14853, USA*
[3]*Department of Physics and Astronomy, Michigan State University, East Lansing, MI 48824, USA*
[4]*These authors contributed equally to the work*
[*]*dantus@msu.edu*

Abstract: Ultrashort pulse generation in the 1600 nm wavelength region is required for deep-tissue biomedical imaging. We report on the characterization and adaptive compression of a multi-soliton output spanning >300 nm from a large-mode area photonic-crystal fiber rod for two separate laser setups. Sub-30 fs pulses are generated by first compressing of each soliton individually, and then followed by coherently combining all of the pulses in the train, which are separated by hundreds of femtoseconds. Simulations of the source, together with amplitude and phase coherence measurements are provided.

OCIS codes: (320.5520) Pulse compression; (320.7100) Ultrafast measurements; (320.5540) Pulse shaping; (060.5295) Photonic crystal fibers; (190.5530) Pulse propagation and temporal solitons.

References and links

1. N. G. Horton, K. Wang, D. Kobat, C. G. Clark, F. W. Wise, C. B. Schaffer, and C. Xu, "In vivo three-photon microscopy of subcortical structures within an intact mouse brain," Nat. Photonics **7**(3), 205–209 (2013).
2. L.-C. Cheng, N. G. Horton, K. Wang, S.-J. Chen, and C. Xu, "Measurements of multiphoton action cross sections for multiphoton microscopy," Biomed. Opt. Express **5**(10), 3427–3433 (2014).
3. F. M. Mitschke and L. F. Mollenauer, "Discovery of the soliton self-frequency shift," Opt. Lett. **11**(10), 659–661 (1986).
4. J. P. Gordon, "Theory of the soliton self-frequency shift," Opt. Lett. **11**(10), 662–664 (1986).
5. S. A. Dekker, A. C. Judge, R. Pant, I. Gris-Sánchez, J. C. Knight, C. M. de Sterke, and B. J. Eggleton, "Highly-efficient, octave spanning soliton self-frequency shift using a specialized photonic crystal fiber with low OH loss," Opt. Express **19**(18), 17766–17773 (2011).
6. K. Wang, N. G. Horton, K. Charan, and C. Xu, "Advanced fiber soliton sources for nonlinear deep tissue imaging in biophotonics," IEEE J. Sel. Top. Quantum Electron. **20**, 6800311 (2014).
7. M. N. Islam, G. Sucha, I. Bar-Joseph, M. Wegener, J. P. Gordon, and D. S. Chemla, "Femtosecond distributed soliton spectrum in fibers," J. Opt. Soc. Am. B **6**(6), 1149–1158 (1989).
8. J. M. Dudley, G. Genty, and S. Coen, "Supercontinuum generation in photonic crystal fiber," Rev. Mod. Phys. **78**(4), 1135–1184 (2006).
9. B. Nie, I. Saytashev, A. Chong, H. Liu, S. N. Arkhipov, F. W. Wise, and M. Dantus, "Multimodal microscopy with sub-30 fs Yb fiber laser oscillator," Biomed. Opt. Express **3**(7), 1750–1756 (2012).
10. X. Gu, L. Xu, M. Kimmel, E. Zeek, P. O'Shea, A. P. Shreenath, R. Trebino, and R. S. Windeler, "Frequency-resolved optical gating and single-shot spectral measurements reveal fine structure in microstructure-fiber continuum," Opt. Lett. **27**(13), 1174–1176 (2002).
11. B. Schenkel, R. Paschotta, and U. Keller, "Pulse compression with supercontinuum generation in microstructure fibers," J. Opt. Soc. Am. B **22**(3), 687–693 (2005).
12. T. C. Wong, M. Rhodes, and R. Trebino, "Single-shot measurement of the complete temporal intensity and phase of supercontinuum," Optica **1**(2), 119–124 (2014).
13. J. Dudley, X. Gu, L. Xu, M. Kimmel, E. Zeek, P. O'Shea, R. Trebino, S. Coen, and R. Windeler, "Cross-correlation frequency resolved optical gating analysis of broadband continuum generation in photonic crystal fiber: simulations and experiments," Opt. Express **10**(21), 1215–1221 (2002).
14. H. Tu, Y. Liu, J. Lægsgaard, U. Sharma, M. Siegel, D. Kopf, and S. A. Boppart, "Scalar generalized nonlinear Schrödinger equation-quantified continuum generation in an all-normal dispersion photonic crystal fiber for broadband coherent optical sources," Opt. Express **18**(26), 27872–27884 (2010).
15. G. Krauss, S. Lohss, T. Hanke, A. Sell, S. Eggert, R. Huber, and A. Leitenstorfer, "Synthesis of a single cycle of light with compact erbium-doped fibre technology," Nat. Photonics **4**(1), 33–36 (2010).

#280146 http://dx.doi.org/10.1364/OE.25.000320
Journal © 2017 Received 4 Nov 2016; revised 23 Dec 2016; accepted 23 Dec 2016; published 5 Jan 2017

Optics EXPRESS

16. V. V. Lozovoy, I. Pastirk, and M. Dantus, "Multiphoton intrapulse interference 4; characterization and compensation of the spectral phase of ultrashort laser pulses," Opt. Lett. **29**, 775–777 (2004).
17. B. Xu, J. M. Gunn, J. M. Dela Cruz, V. V. Lozovoy, and M. Dantus, "Quantitative investigation of the MIIPS method for phase measurement and compensation of femtosecond laser pulses," J. Opt. Soc. Am. B **23**, 750–759 (2006).
18. Y. Coello, V. V. Lozovoy, T. C. Gunaratne, B. Xu, I. Borukhovich, C. Tseng, T. Weinacht, and M. Dantus, "Interference without an interferometer: a different approach to measuring, compressing, and shaping ultrashort laser pulses," J. Opt. Soc. Am. B **25**(6), A140–A150 (2008).
19. V. V. Lozovoy, B. Xu, Y. Coello, and M. Dantus, "Direct measurement of spectral phase for ultrashort laser pulses," Opt. Express **16**(2), 592–597 (2008).
20. K. Wang, T.-M. Liu, J. Wu, N. G. Horton, C. P. Lin, and C. Xu, "Three-color femtosecond source for simultaneous excitation of three fluorescent proteins in two-photon fluorescence microscopy," Biomed. Opt. Express **3**(9), 1972–1977 (2012).
21. J. M. Dudley and S. Coen, "Coherence properties of supercontinuum spectra generated in photonic crystal and tapered optical fibers," Opt. Lett. **27**(13), 1180–1182 (2002).
22. J. M. Dudley and J. R. Taylor, *Supercontinuum Generation in Optical Fibers* (Cambridge University Press, 2010), Chap. 3.
23. V. V. Lozovoy, G. Rasskazov, D. Pestov, and M. Dantus, "Quantifying noise in ultrafast laser sources and its effect on nonlinear applications," Opt. Express **23**(9), 12037–12044 (2015).
24. G. Rasskazov, V. V. Lozovoy, and M. Dantus, "Spectral amplitude and phase noise characterization of titanium-sapphire lasers," Opt. Express **23**(18), 23597–23602 (2015).
25. E. R. Andresen, P. Berto, and H. Rigneault, "Stimulated Raman scattering microscopy by spectral focusing and fiber-generated soliton as Stokes pulse," Opt. Lett. **36**(13), 2387–2389 (2011).
26. K. Wang and C. Xu, "Tunable high-energy soliton pulse generation from a large-mode-area fiber and its application to third harmonic generation microscopy," Appl. Phys. Lett. **99**(7), 071112 (2011).
27. S. Saint-Jalm, E. R. Andresen, P. Ferrand, A. Bendahmane, A. Mussot, O. Vanvincq, G. Bouwmans, A. Kudlinski, and H. Rigneault, "Fiber-based ultrashort pulse delivery for nonlinear imaging using high-energy solitons," J. Biomed. Opt. **19**(8), 086021 (2014).
28. K. A. Walowicz, I. Pastirk, V. V. Lozovoy, and M. Dantus, "Multiphoton intrapulse interference 1; control of multiphoton processes in condensed phases," J. Phys. Chem. A **106**(41), 9369–9373 (2002).
29. V. V. Lozovoy, I. Pastirk, K. A. Walowicz, and M. Dantus, "Multiphoton intrapulse interference II. Control of two- and three-photon laser induced fluorescence with shaped pulses," J. Chem. Phys. **118**(7), 3187–3196 (2003).

1. Introduction

Long-wavelength (1600-1800 nm) femtosecond pulses and the detection of their higher-order nonlinear optical signals such as third-harmonic generation and four-photon excited fluorescence have led to unprecedented accomplishments in deep-tissue biomedical imaging [1,2]. Soliton fission in optical fibers, resulting from anomalous dispersion regime pumping, and consequent soliton self-frequency shift (SSFS) [3–5], has been considered ideal for generating the bandwidth needed for imaging experiments, especially when using large mode area (LMA) fibers or photonic crystal (PC) rods [6]. The low dispersion of an isolated SSFS soliton leads to stable ~70 fs pulses [2,6]. However, when pumped with high-energy, SSFS in a PC rod can produce an output spectrum with bandwidths > 300 nm. The temporal structure of the emitted light consists of a pulse arising from third-order optical nonlinearity, and a train of independent pulses resulting from soliton fission, where each pulse experiences a different spectral shift, dispersion, and time delay [7,8]. Here we use a programmable pulse shaper to characterize, compress and coherently combine this complex multi-soliton source in order to achieve greater peak intensity, bandwidth and shorter pulse durations. Successful compression of these types of sources can lead further advances in multi-photon microscopy because a factor of ~3.16 reduction in the pulse duration results in a 10x enhancement of the third-order nonlinear optical signal, and a ~32x enhancement of the fourth-order optical signal [2,9].

Although characterization of supercontinuum pulses from photonic crystal fibers in the normal dispersion regime is challenging, it has been accomplished [10–14], even down to sub-10 fs compressed pulses [14]. Multi-soliton SSFS sources are particularly difficult to characterize because they consist of multiple solitons, each with a different carrier frequency and group velocity dispersion. Characterization and compression of a multi-soliton output requires the independent characterization and compression of each soliton, followed by

Optics EXPRESS

coherent phase combining of all the solitons into a single coherent pulse. A similar approach to compress individual spectral parts was applied in the study by Gunter Krauss et al. [15]. While accomplishing this manually seems a formidable task, here we take advantage of a broadband pulse shaper and the multiphoton intrapulse interference phase scan (MIIPS) characterization and compression method [16–19]. Results from two different laboratories presented here indicate the approach presented is robust.

2. Experimental setup and results

The experiments reported in this work were carried out in two different laboratories, one at Cornell and one at Michigan State University (MSU). The experimental setup for both laser systems was very similar (Fig. 1). The setup consisted of a pump laser (Cazadero, Calmar Laser) that produced ~500 fs pulses at a central wavelength of ~1550 nm. At Cornell, the laser operated at a repetition rate of 1 MHz, producing 1.3 μJ pulse energy, was coupled into a 37 cm long LMA PC rod (100 μm diameter, NKT Photonics, Denmark). At MSU, the laser operated at a repetition rate of 2 MHz, producing 0.41 μJ pulse energy, was coupled into a 45 cm LMA PC rod (100 μm diameter, aeroCHROME-ROD-MODULE, NKT Photonics, Denmark). The soliton order was calculated to be 14 and 7 for the first and the second laser setups, respectively [8]. This parameter correlates with the ability of input pulses to produce multiple solitons in an optical fiber via the fission process. Dispersion of the rods was anomalous in the spectral range of interest, with a dispersion parameter of ~25 ps/nm/km at 1550 nm. The nonlinear parameter was estimated to be ~0.03 $W^{-1}km^{-1}$. The coupling efficiency into the rod was ~93% for both lasers. A pulse shaper (MIIPS Box 640, Biophotonic Solutions Inc., USA) was used to both measure and correct phase distortions of the rod output using MIIPS [18], and to obtain the interferometric autocorrelation on the pulses. We used pulse shaper to isolate spectrally each of the solitons to characterize their spectral phase, and to adaptively compress them by introducing a phase that cancels the dispersion measured for each soliton. After compression, the pulse shaper was used to synchronize the arrival of each soliton in order to coherently combine them. We compared the autocorrelations measured by the MIIPS with a numerical simulation based on the fundamental spectrum. Second harmonic signal was generated in a 10-μm beta barium borate (BBO) Type I crystal and used as a feedback for the pulse shaper. The phase matching bandwidth of the BBO crystal covered the entire optical bandwidth of the system output.

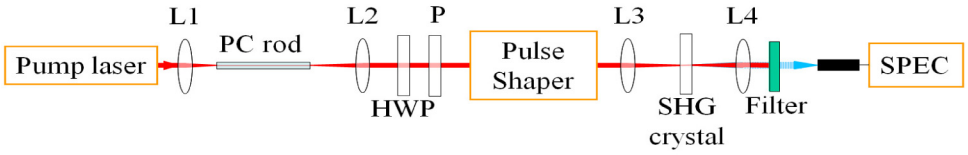

Fig. 1. Schematic of the experimental setup for multi-soliton generation: L1-4, lenses; HWP, half-wave plate; P, polarizer; SPEC, optical spectrum analyzer.

Figures 2(a) and 2(b) show the multi-soliton broadband output spectra for the two laser setups. In both cases we observed two fundamental solitons caused by soliton fission and a blue-shifted pulse caused by four-wave mixing effects [8]. The output spectrum depends on the pump intensity, wavelength-dependent fiber parameters, and a self-induced Raman scattering process. As each soliton propagates in the PC rod, the intrapulse Raman scattering effect and group velocity walk-off separates the solitons from the residual input pump laser and from one another [8,21]. This also reduces the influence of the blue-shifted radiation, resulting in better stability for the longest wavelength soliton. The spectrum in general contains four components: a high intensity modulation instability (MI) region that overlaps with some of the residual input pump pulse, a blue-shifted pulse, and two red-shifted solitons, see Fig. 2. Note that the spectrum in Fig. 2(a) is broader than the one in Fig. 2(b) because of the greater input pulse energy.

Optics EXPRESS

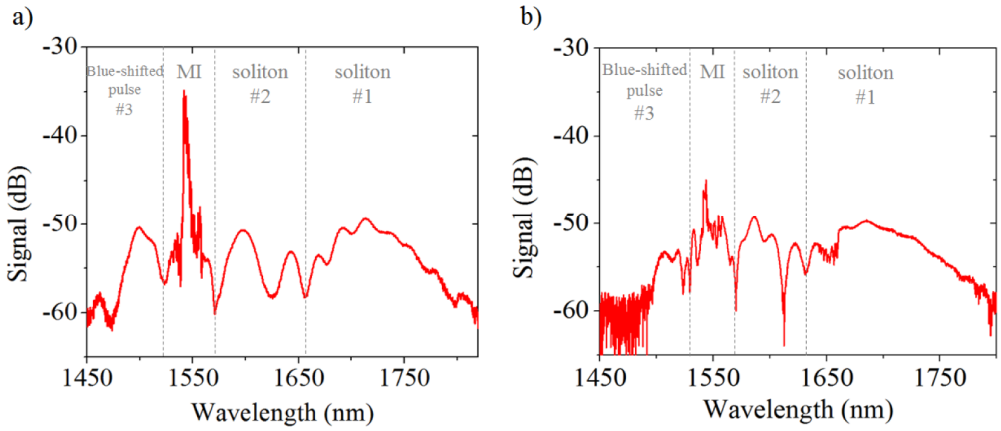

Fig. 2. Multi-soliton spectra of LMA PC rod output in semi-logarithmic scale for (a) 1.3 μJ pump pulse energy and 37 cm long PC rod; and (b) 0.4 μJ pump pulse energy and 45 cm long PC rod.

We performed numerical simulations of the nonlinear pulse propagation. The simulations were based on generalized nonlinear Schrödinger equation (GNLSE), which includes higher order nonlinearity and stimulated Raman scattering [22]. The degree of coherence was determined for 100 pulses coupled to a PC rod with random intensity noise in order to determine the expected output pulse-to-pulse fluctuations [8]. We used the experimentally measured parameters with 1% power fluctuations. Figure 3 (red curves) shows the simulated average spectrum for both laser systems, which are in a good agreement with the experimental spectra. The degree of coherence, calculated as in [8], is shown in Fig. 3 as black curves. The overall coherence is high for the majority of the spectral components with high spectral intensity.

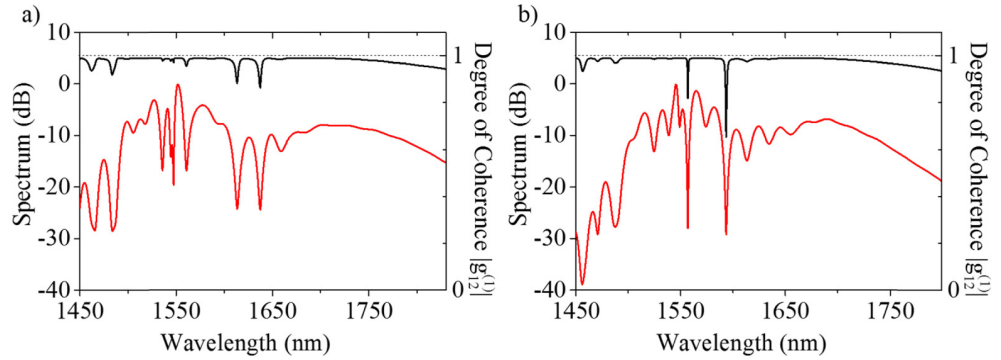

Fig. 3. Average spectrum (left axis, red curve) and degree of coherence (right axis, black curve) calculated for an ensemble of 100 pulses for (a) the first laser system with 1.3 μJ pump pulse energy and 37 cm long PC rod; and (b) the second laser system with 0.4 μJ/pulse and 45 cm long PC rod.

Figures 4(a) and 4(d) show the MIIPS traces obtained for both laser setups. In both cases, the incoherent MI with residual input region between 1540 nm and 1558 nm was blocked with a card at the spatial light modulator in the pulse shaper. In the MIIPS traces the second harmonic generation (SHG) intensity is plotted as a function of both the wavelength and the chirp applied by the pulse shaper [17]. One can distinguish the SHG from each of the two solitons marked as 1 and 2 and from the blue-shifted pulse marked as 3. Two additional signals, labeled as 1 + 2 and 2 + 3, result from sum-frequency generation. Individual compression was accomplished by performing MIIPS on the desired part of the spectrum and

Optics EXPRESS

blocking the non-desired parts at the SLM. This resulted in 57 fs, 155 fs, and 150 fs pulses for the first laser setup and 90 fs, 156 fs and 210 fs for the second laser setup, for spectral regions 1, 2, and 3, respectively. Delay scans for the first laser setup revealed a ~540 fs delay between solitons 1 and 2, and ~120 fs between 2 and 3. Delay scans for the second laser setup showed a 900 fs delay between solitons 1 and 2, and 700 fs between 2 and 3. After the individual solitons were temporally overlapped with each other, the coherent output was close to the transform limited (TL) pulse duration. This was confirmed by the MIIPS traces shown in Figs. 4(b) and 4(e), where most of the SHG intensity is concentrated at zero-chirp. Numerical simulations of the SHG chirp scan based on the experimental spectra for a transform-limited pulse agrees well with the experimental data [Figs. 4(c) and 4(f))], indicating successful compression. Note that MIIPS corrected for the dispersion from all optics in the beam path including the shaper to achieve TL pulses.

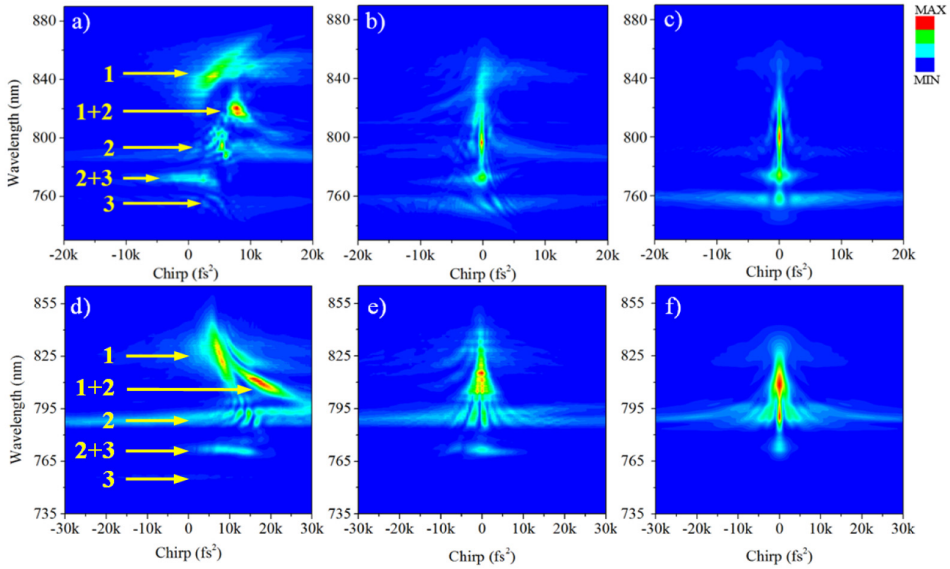

Fig. 4. MIIPS traces showing the SHG intensity as a function of wavelength and spectral chirp: (a)-(c) for 1.3 μJ per pulse and 37 cm long PC rod; (d)-(f) for 0.4 μJ per pulse and 45 cm long PC rod. (a) and (d) before compression, (b) and (e) after compression, (c) and (f) numerical calculation assuming transform-limited pulses based on the input spectra. Each trace was independently normalized.

Frequency-resolved cross-correlation traces of the second laser system output, which used the longer wavelength soliton at 1668 nm as a reference, revealed the time delay among the different output spectral regions (Fig. 5). In Fig. 5(a) one can see that each of the components has a different time delay. For example the delay is 900 fs between solitons 1 and 2, and 700 fs between soliton 2 and the blue-shifted pulse. In Fig. 5(b) we show a corresponding trace after the blue shifted pulse and the two solitons were synchronized, and coherently phase combined. The fundamental spectrum is shown in Fig. 5(c) as a reference and in Fig. 5(d) with the spectral phase composed of individual phase corrections for each pulse and relative delay adjustments. Cross-correlations of the laser source prior to and after compression demonstrate the multi-soliton output with an overall ‘pulse duration’ greater than 1500 fs is compressed to ~30 fs, resulting in a compression factor of ~50.

Optics EXPRESS

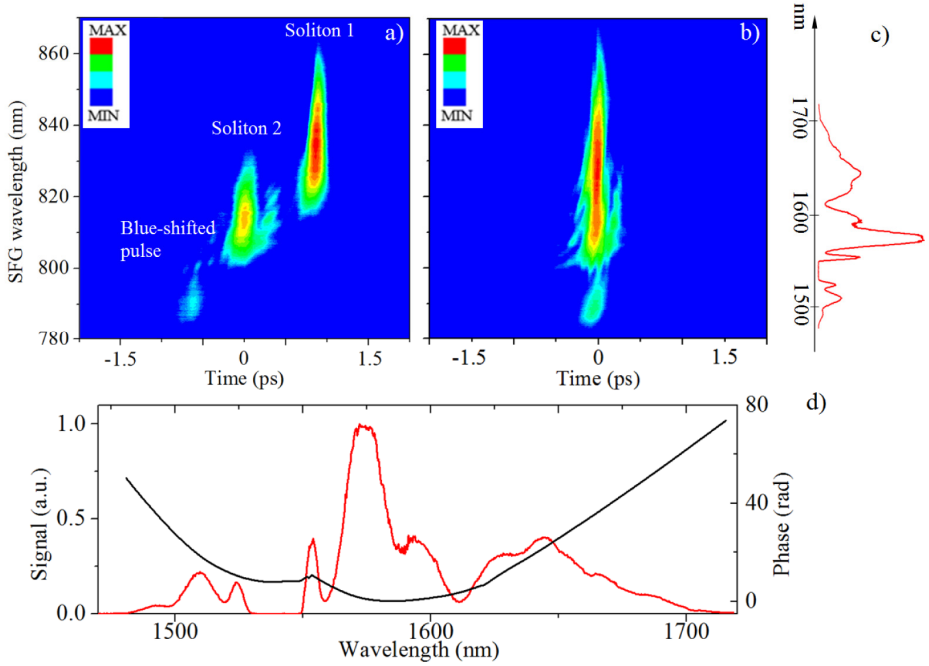

Fig. 5. Frequency-resolved cross-correlation traces of the PC rod output of the second laser system without (a) and with (b) delay compensation. Intensity is plotted on a logarithmic scale. Plots were centered at soliton 2 for symmetry. (c) The fundamental spectrum. Note the wavelength axis of the fundamental spectrum is not linear. (d) The fundamental spectrum and the transform-limited spectral phase.

The integrated SHG intensity was ~3 times greater after the coherent temporal combining for both lasers. The SHG spectra with and without coherent temporal combining and the interferometric autocorrelation of the output, and its numerical simulation, are shown in Figs. 6(a)-6(c) for the first laser system and in Figs. 6(d)-6(f) for the second one. Temporal side lobes in both cases result from the highly structured spectrum. The pulse shape used to calculate the pulse width was determined by fitting the autocorrelation. We found a sech^2shape fits well down to 10% of the amplitude, and a Gaussian function did not fit well below the 50% intensity level. Assuming a sech^2 pulse shape, the full width at half maximum pulse duration was 28 fs and 45 fs for the first and second laser setups, respectively. The energy per pulse and peak power after compression were measured to be 0.3 μJ and 10 MW for the first laser setup, and 0.15 μJ and 3.15 MW for the second laser setup. These energies are almost an order of magnitude higher than the energy that has been used for *in vivo* three photon microscopy [1].

Optics EXPRESS

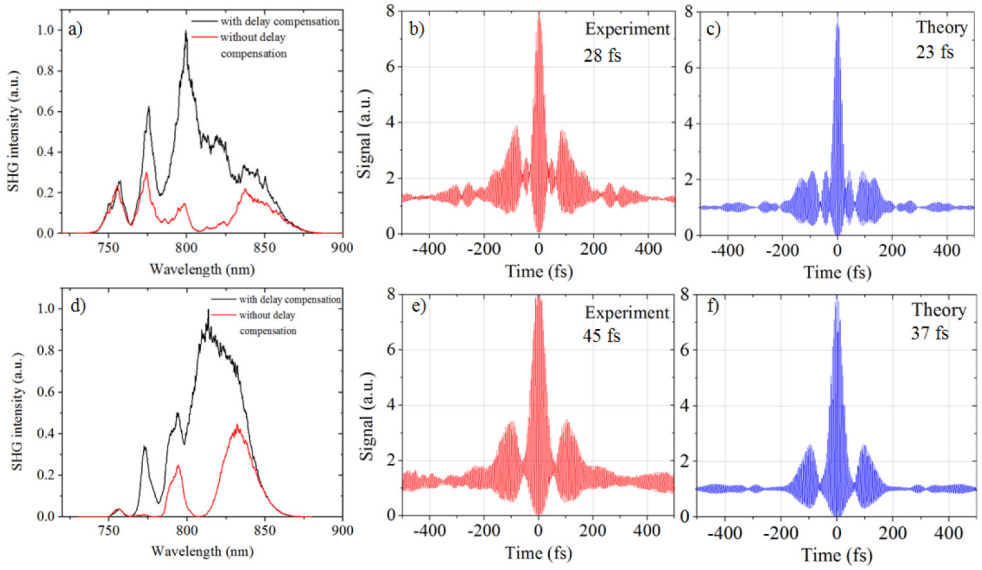

Fig. 6. Results after compresssion. (top row) the first laser setup, (bottom row) the second laser setup. (a) and (d) the normalized SHG spectra before (red curve) and after (black curve) coherent temporal combining. (b) and (e) experimental interferometric autocorrelations. (c) and (f) theoretical interferometric autocorrelations.

In order to characterize the pulse-to-pulse noise of the laser source, namely spectral amplitude and phase fluctuations, we used the fidelity parameter [23]. The fidelity measurement involves a calculation of the ratio between theoretical and experimental normalized intensities of the second harmonic signal as a function of linear chirp. In theory, an ideal laser has a fidelity parameter of 1.0. For comparison, Ti:Sapphire oscillators can achieve a fidelity parameter greater than 0.9, while fiber lasers usually operate at a fidelity parameter of 0.8-0.9. It has been shown that spectral phase and amplitude noise result in distinct fidelity signatures [23,24]. Figure 7(a) shows the fidelity measurement for the multi-soliton source of the first laser setup. A fidelity parameter of ~0.48 is estimated as the asymptotic value (after ± 15k fs^2) of our measurements. The second laser system had a 10% greater fidelity, which resulted from a few technical improvements such as isolating the laser from ambient airflow, shorter optical path between the pump laser and PC rod. The relatively low fidelity values observed for multi-soliton compression indicate pulse-to-pulse spectral breathing in the output [23]. The shape of the fidelity curve indicates the phase of the output spectrum is stable. Spectral breathing results from instabilities from the pump laser, which degrades the coupled peak intensity in the PC rod and causes the greater than 300 nm bandwidth to fluctuate. This behavior agrees with previous studies on the coherent properties of supercontinuum in a PC rod in the anomalous dispersion regime [21]. Fidelity measurements of the isolated (longest wavelength) soliton for the first laser system (~100 nm bandwidth) [Fig. 7(b)] gave an asymptotic value of ~0.9, confirming high pulse quality and coherence. Typically, this long wavelength soliton is used for Raman microscopy and multiphoton microscopy [25–27].

Optics EXPRESS

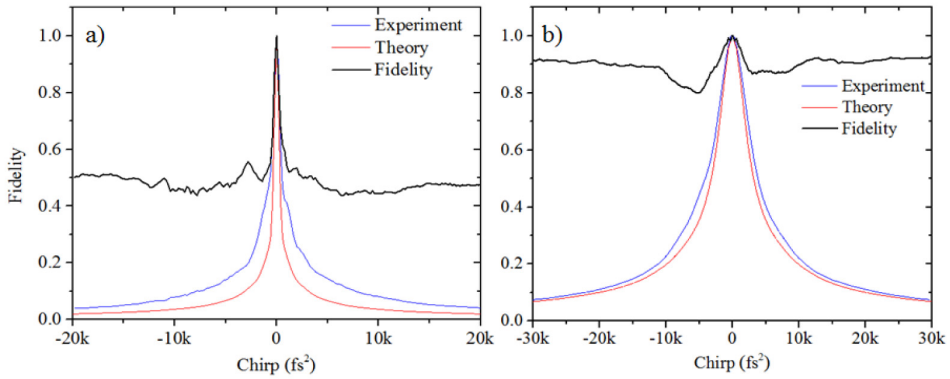

Fig. 7. Fidelity measurements for the multi-soliton source of the first laser system after compression obtained (a) for the entire spectrum and (b) for the isolated long-wavelength soliton.

In order to further test the phase stability of the coherently combined multi-soliton output, we scanned the phase of one of the solitons with respect to the rest of the output. The phase of the long-wavelength soliton was varied from –2π to 2π using the pulse shaper in 0.5 rad increments [Fig. 8(a)]. Multiphoton intrapulse interference [28,29] modulates the sum frequency generation signal with complete destructive interference at values of ± π as shown in Fig. 8(b). The modulation depth, 100% theoretically, indicates a high level of phase coherence between different parts of the spectrum. Detecting the second harmonic signal at the wavelengths corresponding to sum frequency generation (Fig. 8(b), blue arrows) resulted in a sinusoidal dependence as predicted by theory [Figs. 8(c) and 8(d)]. In the Fig. 8(e) a sinusoidal phase scan was performed. The periodic spectral phase, $\varphi(\omega) = \alpha \cos[\gamma(\omega - \omega_0) - \delta]$ was applied by the pulse shaper, where $\alpha = 2$, $\gamma = 40$ fs and δ was scanned from 0 to 2π. The equidistant parallel lines are the signatures of TL pulses [16]. For a TL output one can clearly see traces predicted by theory. The reproducibility of the phase scan and MIIPS traces was checked over a day operation of the laser. This behavior confirms good long term phase stability, which is supported by the analysis of the shape of the fidelity curve in Fig. 7.

Optics EXPRESS

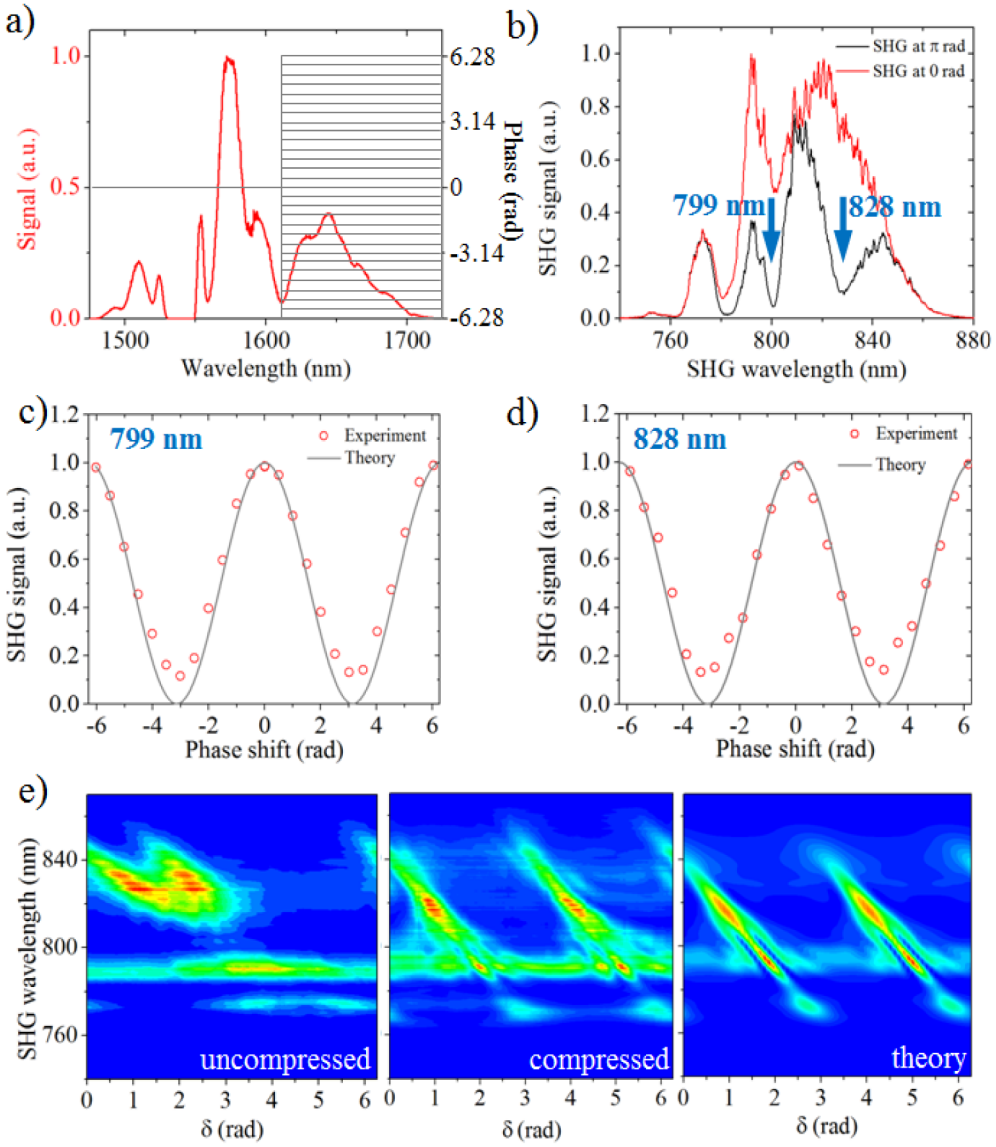

Fig. 8. Phase coherence tests of the compressed multi-soliton source. (a) The fundamental spectrum and the phase from –2π to 2π applied to the longest-wavelength soliton. (b) Second harmonic spectra at 0 rad (red) and π rad (black). The arrow shows the wavelengths that appeared due to the sum frequency generation. Normalized experimental and theoretical results from a phase shift scan for 799 nm (c) and 828 nm (d). (e) MIIPS scans for both uncompressed and compressed pulses, as well as numerical simulations.

3. Conclusion

In summary, we reported the successful characterization, compression and coherent combining of multiple solitons from a large mode area photonic crystal fiber rod using a MIIPS enabled pulse shaper for two separate laser setups. Pulses as short as 28 fs were obtained, although in such a case some spectral breathing was identified based on fidelity (coherent and pulse-to-pulse stability properties) measurements and degree of coherence simulations. When the long-wavelength soliton was isolated, pulses as short as 57 fs were measured, and these pulses had higher fidelity. The factor of two shorter pulses would result

Optics EXPRESS

in a factor of 8 or 16 enhancement in the signal for third- or fourth-order nonlinear optical processes. The shaper-based compression scheme used here should work well for a fiber output containing more than 3 independent pulses. We conclude that compression of complex multi-soliton sources offers a path to short pulse generation at wavelengths in the ~1.5-1.9 μm wavelength region where it can be used for deep-tissue biomedical imaging based on third-harmonic generation, as well as three- and four-photon excited fluorescence imaging modalities.

Funding

Department of Homeland Security, Science and Technology Directorate (DHS-ST) (HSHQDC-15-C-B0002); National Institutes of Health (NIH) (R01EB014873, R01EB017274).